NUMERICAL STUDY WITH EXPERIMENTAL COMPARISON OF PRESSURE WAVES IN THE AIR INTAKE SYSTEM OF AN INTERNAL COMBUSTION ENGINE

Carlos E G Falcão, smkadu@yahoo.com.br
Mechanical Engineering Graduate Program – Federal University of Rio Grande do Sul – UFRGS – Porto Alegre, RS, Brazil

Sérgio M Hanriot, hanriot@pucminas.br
Mechanical Engineering Department – Pontifical Catholic University of Minas Gerais – PUCMinas – Belo Horizonte, MG, Brazil

Horácio A Vielmo, vielmoh@mecanica.ufrgs.br
Mechanical Engineering Department – Federal University of Rio Grande do Sul – UFRGS – Porto Alegre, RS, Brazil

Abstract. *The work investigates the pressure waves behavior in the intake system of an internal combustion engine. For the purpose of examining this problem, it was chosen an experimental study in order to validate the results of the present simulation. At the literature there are several experimental studies, and some numerical simulations, but the most of the numerical studies treat the problem only in one dimension in practical problems, or two dimensions in specific problems. Using a CFD code it is possible to analyze more complex systems, including tridimensional effects. The pulsating phenomenon is originated from the periodic movement of the intake valve, and produces waves that propagate within the system. The intake system studied was composed by a straight pipe connected to a 1000 cc engine with a single operating cylinder. The experiments were carried out in a flow bench. In the present work, the governing equations was discretized by Finite Volumes Method with an explicit formulation, and the time integration was made using the multi-stage Runge-Kutta time stepping scheme. The solution is independent of mesh or time step. The numerical analysis presents a good agreement with the experimental results.*

Keywords: *ICE air intake system, Pressure wave, CFD transient analysis*

1. INTRODUCTION

The treatment of the pressure waves problems has immediate practical interests, for example, the air intake system of an internal combustion engine. In the internal combustion engines the pulsating phenomenon is originated from the periodic movement of the intake valve and piston, and produces waves that propagate within the system. If the peak of pressure is in the intake valve at its closure, the volumetric efficient increases.

Morse et al. (1938) studied the influence of acoustic vibrations derived from the movement of the valves of an internal combustion engine, and state that they can decrease or increase the performance of equipment.

Benson and Winterbone (1989) said that in case of a real engine, when the pressure pulse reaches the intake valve at its closure, there is an increase of amount of air admitted. Previously, Benson had successfully used the numerical method of characteristics to simulate this kind of problem.

In the field of Finite Volumes treatment, Yasunobu et al. (2002) showed the numerical results obtained by using the TVD (Total Variation Diminishing), second order scheme to solve the conservation equations. It considers a tube with a high pressure closed chamber, separated by a diaphragm of another chamber, at ambient pressure, opened to the external environment. It is shown that the maximum variation of the wave of compression or expansion depends on the initial difference of pressures between the chambers, but is independent of their size.

William-Louis et al. (2004) investigated, using the Finite Volumes Method, the output of an air duct, which has inside a high pressure chamber separated by a diaphragm of the remaining tube. However, takes into account different considerations at the exit of the tube. The time step was set at 2.08E-06 seconds, with a cell size of 12E-4 meters, the accuracy of the solution is second order both in space and time. They compared the numerical results with experimental work reported, and also with analytical results developed by Brown and Vardy (1994). They concluded that the overall pressure waves are the superposition of waves that propagate in their own output and reflecting on the corners of the output. The analytical calculation was confirmed, showing that the amplitude of transverse wave at the output flange is not much more important than the flange, although the analytical calculations not represent well the reality of the first few seconds, since they underestimate the first pressure gradients.

When it is desired to capture the pressure waves phenomenon in low Mach number compressible flows, the system of equations is very stiff, and the numerical scheme must be manipulated to decrease the great disparities between time and/or length scales usually caused by the differences between acoustic and convective velocities. When it is done by using a precondition matrix, the numerical scheme loses its accuracy in time. The preconditioning matrix used in the present work was exposed by Weiss (1995). To return the accuracy in time, the dual time-stepping scheme was used (Merkle (1987)).

The work of Sod (1978) provides exact solutions using various methods to the problem of pressure waves propagation, creating a basis for comparison for future validations.

Hanriot (2001) conducted experiments to evaluate the reflections in an air intake duct. The experimental methodology, all performed in a flow bench, looked at the waves in the duct with and without resonator, was assessed at different speeds and lengths of pipelines. With the resonator, different volumes of resonance chamber could be analyzed.

In the present work, the validation of the program is presented and a comparison between the numerical and experimental investigation presented by Hanriot (2001) is made. As the velocity of the phenomena is very high, the time step must be very small, in order to reach the stability criteria used in the program. By this way, it is preferable to use an explicit formulation, because it needs less memory to perform the calculations, and according to Al-Falahi et al. (2010) and Star CCM+ User Guide (2010), it is necessary to use the multi-stage Runge-Kutta time stepping scheme to make the time-integration. The coupled form was used because it can treat de velocity of propagation more realistically than the segregated form. This formulation was also advised by Star CCM+ User Guide (2010) with the argument that it must be used in case where the pressure waves are more important.

2. CASE DESCRIPTION

The experimental basis of the numerical study is the investigation made by Hanriot (2001). It was chosen the case that treat about an approximately 2 meters long admission tube, with a resonator in a particular position. The resonator and its connection with de tube have their dimensions shown in Fig. 1. The engine rotation is 600 rpm. The problem to be solved has a three-dimensional domain with the intention to study the effects of pressure waves over the numerical code, using an experimental procedure the way that the results can be compared. Obviously, the domain has the same geometry of the used in experimental procedure carried out by Hanriot (2001). It was chosen a single case of all experimented, as already commented. The geometry is shown in Fig. 1.

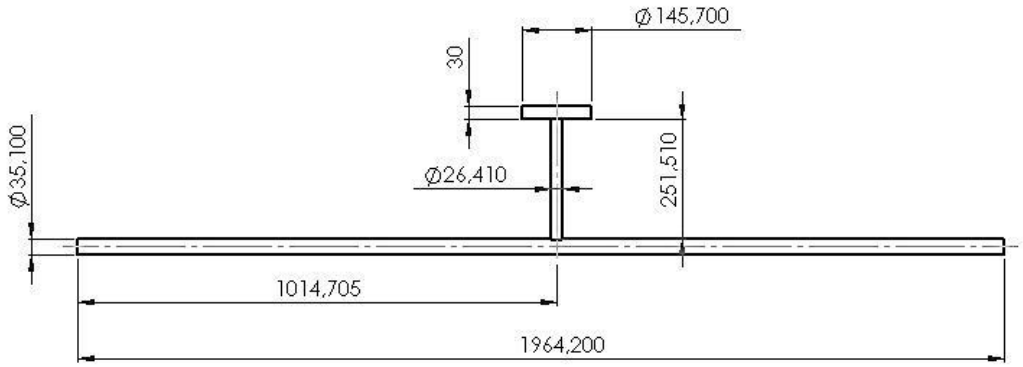

Figure 1. Domain of the problem (mm).

2.1. Boundary and initial conditions

The initial condition comes from a previous cycle simulated, the way that a result can be reached with no perturbation of the resonating phenomenon or distortions caused by the fluid at rest (as the fluid velocity is unknown, the first cycle starts with the fluid velocity zero to generate the initial condition to the second cycle). The entire domain has wall condition with slip treatment. The intake valve region has experimental pressure that varies according the time. The other extremity is opened to the atmosphere (stagnation pressure condition).

2.1.1 Wall condition

To solve this problem, all boundaries have the same wall condition. Velocity, pressure and temperature (inviscid flow) for slip walls are defined by extrapolating the parallel component in the adjacent cell using reconstruction gradients.

2.1.2 Pressure Outlet Condition

The boundary pressure p_f is specified. When the flow changes its direction, the boundary pressure is assumed to be given by:

$$p_f = p_{specified} - \frac{1}{2}\rho_f |\boldsymbol{v}_n|^2 \quad (1)$$

where $\boldsymbol{v}_n$ is the normal component of the boundary inflow velocity. This approach discourages backflow from occurring. Problems arise when flow recirculates at the pressure outlet boundary, in which case that boundary is no longer a real outlet. To prevent this, the dynamic head is added to pressure only on the faces where recirculation occurs. In this case, the boundary face velocity and the temperature are extrapolated from the interior using reconstruction gradients.

2.1.3 Stagnation Inlet

About the velocity, the boundary face velocity magnitude is obtained from:

$$\boldsymbol{v}_f = \sqrt{2C_p(T_{tf} - T_f)} \tag{2}$$

where C_p is the specific heat, T_{tf} is the total temperature and T_f is the static temperature. The boundary face total pressure p_{tf} is specified. For a subsonic flow p_f is extrapolated from the adjacent cell using reconstruction gradients. The boundary face total temperature T_{tf} is specified, and the static temperature T_f is obtained as follows:

$$T_f = \frac{T_{tf}}{(P_{tf}/P_f)^{R/C_p}} \tag{3}$$

where P_{tf} is the total pressure, P_f is the static pressure, R is the ideal gas constant.

2.2. Mathematical Model

2.2.1 The governing equations

The basic flow and energy equations are presented in their coupled form for a compressible and inviscid flow. The Navier-Stokes equations in Cartesian integral form, for an arbitrary control volume V, with differential surface area $d\boldsymbol{a}$ as showed in Star CCM+ User Guide (2010), may be written:

$$\frac{d}{dt}\int_V \boldsymbol{W}_\chi dV + \oint[\boldsymbol{F} - \boldsymbol{G}]d\boldsymbol{a} = 0 \tag{4}$$

where:

$$\boldsymbol{W} = \begin{pmatrix} \rho \\ \rho\boldsymbol{v} \\ \rho E \end{pmatrix} \tag{5}$$

$$\boldsymbol{F} = \begin{pmatrix} \rho(\boldsymbol{v} - \boldsymbol{v}_g) \\ \rho(\boldsymbol{v} - \boldsymbol{v}_g) \otimes P\boldsymbol{I} \\ \rho(\boldsymbol{v} - \boldsymbol{v}_g)\boldsymbol{H} \otimes P\boldsymbol{v}_g \end{pmatrix} \tag{6}$$

$$\boldsymbol{G} = \begin{pmatrix} 0 \\ \boldsymbol{T} \\ \boldsymbol{T}\boldsymbol{v} + \boldsymbol{q}" \end{pmatrix} \tag{7}$$

and ρ, $\boldsymbol{v}$, E, and P, are the density, velocity, total energy per unit mass, and pressure of the fluid, respectively. T is the viscous stress tensor, $\boldsymbol{q}"$ is the heat flux vector, and $\boldsymbol{v}_g$ is the grid velocity vector. Total energy E is related to the total enthalpy H by:

$$E = H + \frac{P}{\rho} \tag{8}$$

where:

$$H = h + \frac{|\boldsymbol{v}|^2}{2} \tag{9}$$

and $h = C_p T$.

2.2.2 Preconditioned equations

To provide efficient solution of compressible flow at all speeds, a preconditioning matrix $\boldsymbol{\Gamma}$ is added:

$$\boldsymbol{\Gamma}\frac{\partial}{\partial t}\int_V \boldsymbol{Q}dV + \oint[\boldsymbol{F}-\boldsymbol{G}]\cdot d\boldsymbol{a} = 0 \tag{10}$$

and:

$$\boldsymbol{\Gamma} = \begin{bmatrix} \Theta & 0 & \rho_T \\ \Theta\boldsymbol{v} & \rho\boldsymbol{I} & \rho_T\boldsymbol{v} \\ \Theta H-\delta & \rho\boldsymbol{v} & \rho_T H+\rho C_p \end{bmatrix} \tag{11}$$

where:

$$\boldsymbol{Q} = [P\boldsymbol{v}T]^T \tag{12}$$

is the dependent vector of primary variables. ρ_T is the derivative of density with respect to temperature at constant pressure, and δ = 0 or 1. For an ideal gas $\rho_T = -\frac{P}{RT}$, δ = 1 and this matrix becomes a member of Turkel's family of preconditioners. The parameter Θ is given by:

$$\Theta = \left(\frac{1}{U_r^2}\right) - \left(\frac{\rho_T}{\rho C_p}\right) \tag{13}$$

and:

$$U_r = max\left(|\boldsymbol{v}|, \nu/\Delta x, \epsilon\sqrt{\delta P}/\rho, U_{r\,min}\right) \tag{14}$$

where Δx is the inter-cell length scale over which the diffusion occurs and δP is the pressure difference between adjacent cells. For compressible flows, U_r is further limited to local acoustic speed *c*. The term ϵ is 10^{-3}, and ensure the stability.

2.2.3 Numerical scheme

The flow domain is replaced by a finite number of control volumes, using a trimmed mesh in Fig. 2.

Figure 2. Used mesh and a zoom to better visualization.

The trimmed cells mesher provides a robust and efficient method of producing a high quality grid for both simple and complex mesh generation problems. It combines a number of highly desirable meshing attributes in a single meshing scheme like explained in Star CCM+ User Guide (2010). By this way, the preconditioned equations in discrete form can be demonstrated. Applying Eq. (10) to a cell-centered control volume *n*, it raises the following discretized system:

$$V_n\boldsymbol{\Gamma}_n\frac{\partial Q_n}{\partial t} + \sum_f\left(\boldsymbol{f}_f + \boldsymbol{g}_f\right)\cdot\boldsymbol{a} = 0 \tag{15}$$

where the summation is over the faces defining cell-n, $\boldsymbol{f}_f$ and $\boldsymbol{g}_f$ are the inviscid and viscous fluxes through face-*f*. V_n is the volume of cell-n and $\boldsymbol{\Gamma}_n$ is the preconditioning matrix evaluated in cell-n.

The explicit integration is based on a multi-stage Runge-Kutta scheme. In this case the Courant number is typically limited to one. This restriction is much more severe than the implicit integration scheme, although much less storage will be required for the same size problem. In this case the size of the time-step is determined automatically by the solver such that one value satisfies the Courant condition at all points (that is, the minimum allowable time-step is used everywhere).

2.2.4 Time step calculation

The local time-step (seconds) is computed by consideration of the Courant number and Von Neumann stability conditions:

$$\Delta t = min\left(\frac{CFL\,V}{\lambda_{max}}, \frac{\sigma \Delta x^2}{\nu}\right) \tag{16}$$

where *CFL* is the Courant number (dimensionless), *V* is the cell volume (m³), σ is the Von Neumann number (σ ≈ 1), Δx is a characteristic cell length scale (m) and ν is kinematic viscosity (m²/s). λ_{max} is the maximum eigenvalue of the system as follows:

$$\lambda_{max} = (\boldsymbol{u} \cdot \boldsymbol{a}) + c|\boldsymbol{a}| \tag{17}$$

where $\boldsymbol{u}$ is velocity and c is the speed of sound.

2.2.5 The Runge-Kutta scheme

An important family of time-integration techniques which are of a high order of accuracy, explicit but non-linear and limited to two time levels is provided by Runge-Kutta methods. Compared with the linear multi-step method, the Runge-Kutta schemes achieve high orders of accuracy by sacrificing the linearity of the method but maintaining the advantages of the one-step method, while the former are basically of a linear nature but achieve great accuracy by involving multiple time steps, as explained in Hirsch (2007).

Jameson et al. (1981) explain that an explicit multi-stage time-stepping scheme may be used to discretize the time-derivative in Eq.(10). The solution is advanced from time t to $t + \Delta t$ time with an *m*-stage Runge-Kutta scheme, given by:

$$\boldsymbol{Q}^{(0)} = \boldsymbol{Q}_t$$

$$\boldsymbol{Q}^{(i)} = \boldsymbol{Q}^{(0)} - \alpha_i \Delta t \boldsymbol{\Gamma}^{-1} R^{(i-1)}$$

$$\boldsymbol{Q}_{t+\Delta t} = \boldsymbol{Q}^{m} \tag{18}$$

i = 1, 2, 3, ...m is the stage counter for the *m*-stage scheme and α_i is the multi-stage coefficient for the *i*th stage. In this work, it was used the 5-stage scheme of Runge-Kutta method, and the coefficients founded in the literature are:

$\alpha_1 = 1/4$, $\alpha_2 = 1/6$, $\alpha_3 = 3/8$, $\alpha_4 = 1/2$, $\alpha_5 = 1$.

The residual $R^{(i)}$ is computed from the intermediate solution $\boldsymbol{Q}^{(i)}$, and is given by:

$$R^{(i)} = \frac{1}{V}\sum_f \left\{\boldsymbol{f}\left(\boldsymbol{Q}^{(i)}\right) - \boldsymbol{g}\left(\boldsymbol{Q}^{(i)}\right)\right\} \tag{19}$$

The residual is just a resource to be able to raise the time step without causing instability. The residual for cell-i is filtered using a Laplacian operator.

$$\bar{\boldsymbol{r}}_i = \boldsymbol{r}_i + \varepsilon \sum_{neighbors}\left(\bar{\boldsymbol{r}}_j - \bar{\boldsymbol{r}}_i\right) \tag{20}$$

This equation is used with a Jacobi iteration:

$$\bar{\boldsymbol{r}}_i^m = \frac{r_i^0 + \varepsilon \sum_{neighbors}\left(\bar{\boldsymbol{r}}_j^{(m-1)}\right)}{1 + \varepsilon \sum_{neighbors}(1)} \tag{21}$$

where r_i^0 represents the original (unsmoothed) residuals and $\bar{r}_i^m$ represents the smoothed residuals after iteration *m*. ε is the under-relaxation factor.

2.2.6 The treatment of inviscid fluxes

The inviscid fluxes are evaluated by using the Weiss-Smith preconditioned Roe's flux-difference splitting scheme [Weiss et al. (1995) and Weiss et al. (1999)]. The $\boldsymbol{f}_f$ term contains characteristic information propagating through the domain with speed and direction according to the eigenvalues of the system. By splitting this term, each part contains the characteristic information, and upwind differencing the split fluxes in a manner consistent with their corresponding eigenvalues, the following expression for the value of the flux at each face is obtained:

$$\boldsymbol{f}_f = \frac{1}{2}(\boldsymbol{f}_0 - \boldsymbol{f}_1) - \frac{1}{2}\boldsymbol{\Gamma}|\boldsymbol{A}|\Delta\boldsymbol{Q} \tag{22}$$

"0" and "1" refer to the cells on either side of face-*f*.

$$\Delta\boldsymbol{Q} = \boldsymbol{Q}_1^r - \boldsymbol{Q}_0^r \tag{23}$$

where $\boldsymbol{Q}_1^r$and $\boldsymbol{Q}_0^r$ are the solution vectors from cell-1 and cell-0 interpolated to the face using reconstruction gradients.

$$|\boldsymbol{A}| = \boldsymbol{M}|\Lambda|\boldsymbol{M}^{-1} \tag{24}$$

where $|\Lambda|$ is the diagonal matrix of eigenvalues and $\boldsymbol{M}$ is the modal matrix that diagonalizes $\boldsymbol{\Gamma}^{-1}\frac{\partial \boldsymbol{f}}{\partial \boldsymbol{Q}}$. By using these reconstructed solution vectors, the discretization scheme becomes formally second-order accurate. It can be viewed as a second-order central-difference plus an added matrix dissipation. The added matrix dissipation term is not only responsible for producing an upwinding of the convected variables, and of pressure and flux velocity in supersonic flow, but it also provides the pressure-velocity coupling required for stability and efficient convergence of low-speed and incompressible flows.

2.2.6 The Dual Time-Stepping Scheme

The preconditioning matrix deteriorates the temporal accuracy. To return the accuracy in time the dual time-stepping scheme is implemented in the numerical scheme, as shown:

$$\frac{\partial}{\partial t}\int \boldsymbol{W}dV + \boldsymbol{\Gamma}\frac{\partial}{\partial \tau}\int_V \boldsymbol{Q}dV + \oint[\boldsymbol{F} - \boldsymbol{G}]\cdot d\boldsymbol{a} = 0 \tag{25}$$

Here it was introduced a pseudo-time derivative. The time-dependent (physical-time) is discretized in an implicit fashion by means of a second order accurate, three point backward difference in time. This scheme added to the Runge-Kutta scheme provides an algorithm that drives the pseudo-time derivative term to zero.

3 VALIDATION OF THE CFD CODE

To ensure de capability of the CFD code to solve this kind of problems and capture shock effects, the code has been validated against an exact solution for Inviscid Flow in Shock Tube.

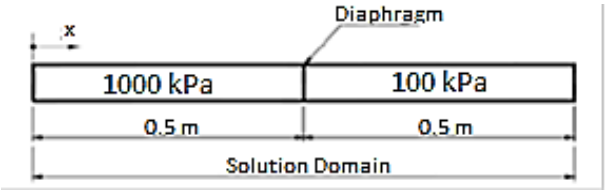

Figure 3. Solution domain for validation

The present CFD solution is compatible with the solution of Sod problem, and is also compatible with the analytical solution of Star CCM+ User Guide (2010). The Sod problem is essentially one-dimensional problem with domain $0 \leq x \leq 1$ and a discontinuity in a $x = 0.5$, that separates two regions at pressure ratio of 10. It was found a solution in the work of Al-Falahi et al. (2010) that is compared with the exact solution found in Sod (1978). The configuration used in Al-Falahi et al. (2010) was: P(left)=1; P(right)=0.1; ρ(left) = 1; ρ(right)=0.125; u(left)=0; u(right) = 0.

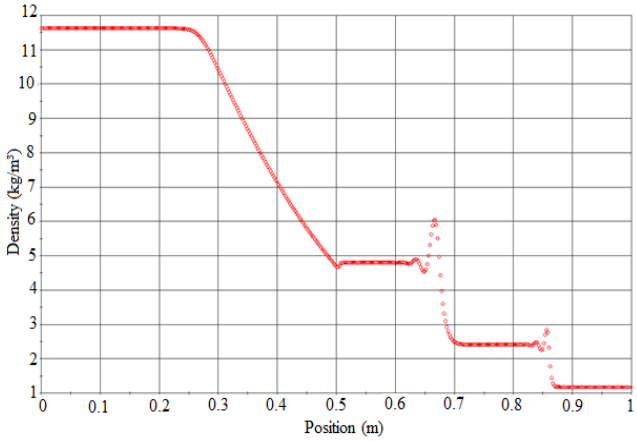

Figure 4. Present solution at 0.64ms.

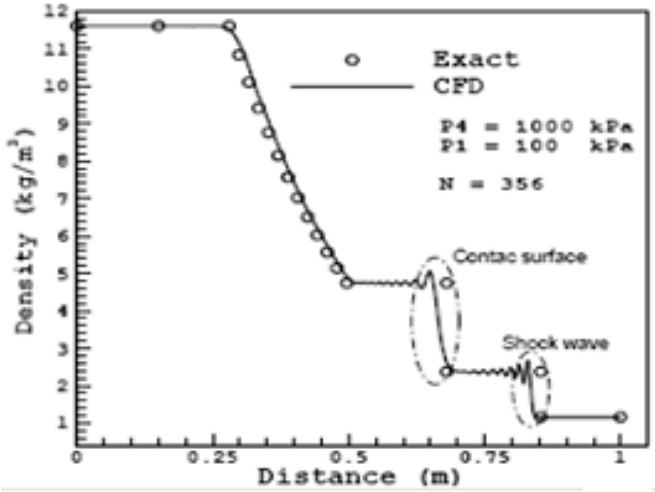

Figure 5. Exact solution and CFD solution of Al-Falahi et al. (2010).

It can be observed that the two physical phenomena in these simulations are totally compatible. That oscillation in the "contact surface" and "shock wave" surface rises because the residual $R^{(i)}$ is considered in the numerical model. The comparison basis uses this term too. Without the residual, the solution is also acceptable, and these oscillations disappear. The residual is just a resource to be able to raise the time step without causing instability. This numerical oscillations decrease as the mesh is refined.

The velocity of the pressure wave is proportional to the speed of sound in the air, at the same conditions:

$$c = \sqrt{kRT} \pm \boldsymbol{v}_{fluid} \tag{26}$$

where k is the ratio of specific heats at constant pressure, R is the ideal gas constant, T is the temperature and $\boldsymbol{v}_{fluid}$ is the velocity of the flow.

A monitoring point at 0.35 m from the initial discontinuity, begins to change its the pressure at 5.76E-4 seconds of simulation. The flux that is established due to pressure ratio in this case reaches its "terminal" velocity for this pressure ratio, about 280 m/s. It gives us a velocity of pressure wave about 327 m/s. Approximately 6% lower than the theoretical speed of sound that would be 347 m/s.

4 EXPERIMENTAL PROCEDURE

The experimental procedure was carried out by Hanriot (2001). In the experimental work, it was used a flow bench composed by a blower that provides the air flow to the intake system. The valves of the combustion chamber are driven by an electrical motor that controls the camshaft speed. The movement of the valves gives rise to a series of pressure waves, which were read at different positions through the use of pressure transducers. The original experimental work collected all data at different rotation, different tube length, different position of the resonating cavity and different chamber volume. A simplified arrangement is shown in Fig.6.

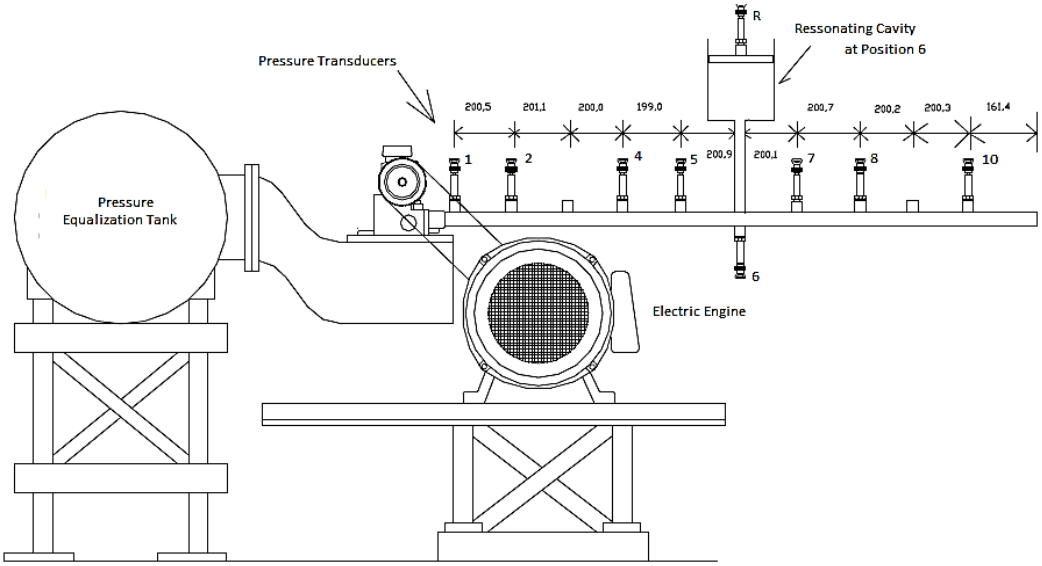

Fig.6. Schematics of intake pipe with Helmholtz resonator.

In the present work, it was chosen a single case with the following configuration: Camshaft rotational speed at 600 rpm, the resonator at position 6 with internal chamber at 30 mm height. All other dimensions are illustrated in Fig.1.

5. RESULTS AND DISCUSSION

For all the results, it was reached the independency of mesh size and time step. To discuss the results several images of the simulation will be shown. Figures 7 to 9 show a very good agreement between the numerical and experimental results. The pressure waves have the same profile in most instants, even in most distant position like position 10.

The position R would be the more critical because it is after an abrupt change in direction, and in case of resonator studies in air intake system of ICE (internal combustion engines), the pressure at this point is very important. The position R is shown in Fig.10, and presents very good agreement with the experimental results also. At this point the pressure has the same behavior in both the experimental method as the Finite Volumes Method.

At the starting cycle (fluid at rest, cycle used like initial condition), the resonating effects are more clear and the graphic become very irregular. In the second cycle, the behavior stabilizes and the graphic become uniform and its profile matches the experimental. At all points measured (Fig. 6), the results matched successfully. In this work only a few points were selected to illustrate the results. The intake valve behavior is shown in the Fig. 11.

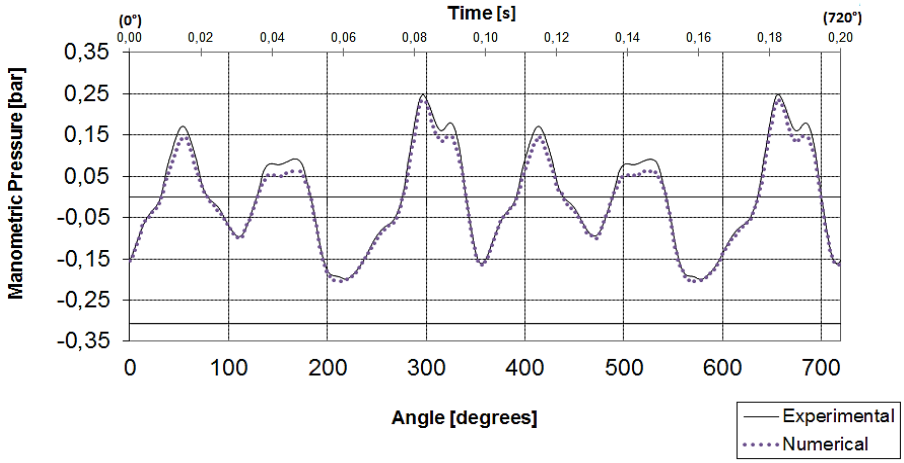

Figure 7. Pressure at position 2.

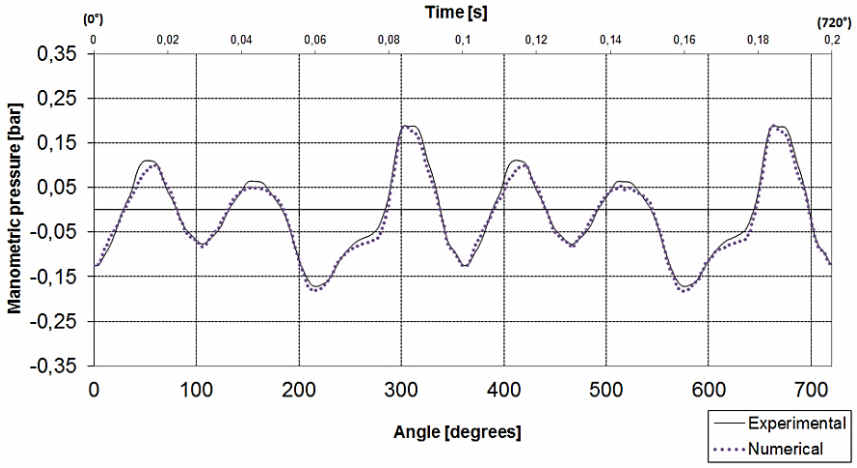

Figure 8. Pressure at position 5.

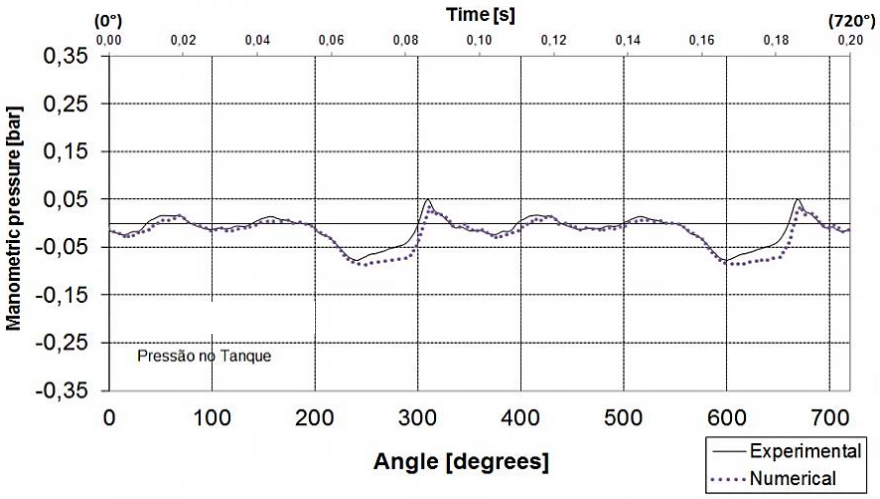

Figure 9. Pressure at position 10.

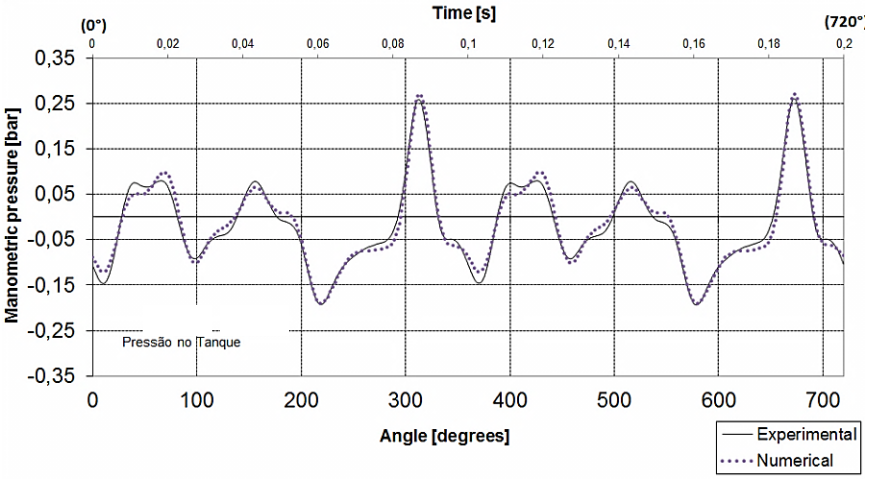

Figure 10. Pressure at position R.

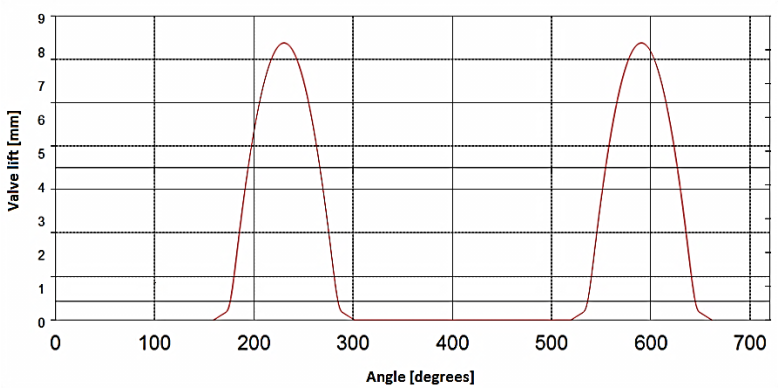

Figure 11. Valve lift versus camshaft angle.

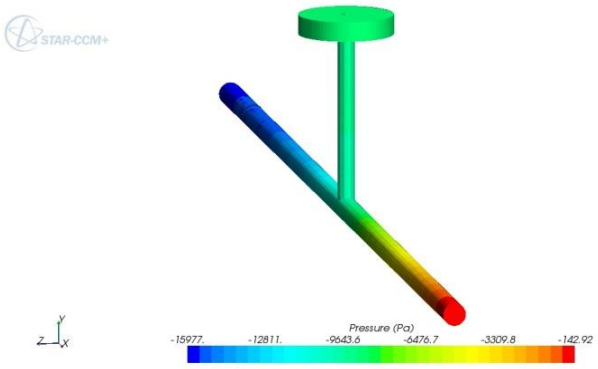

Figure 12. Pressure field at the end of the simulation.

Figure. 12 shows an example of three-dimensional domain and it's plotted the pressure field showing the capability of the code cover the three dimensions. The three-dimensional behavior is usually neglected because the pressure is calculated with other simplified methods. Using the Finite Volumes Method as in this code, these very important effects can be studied in complex geometries.

6. CONCLUSIONS

The work investigates the pressure waves behavior in the intake system of an internal combustion engine and made a comparison between the experimental and numerical results. The pressure at the valve was measured and inserted as a boundary condition in the simulation to study numerically the pressure waves along the geometry. The code presented very good results, capturing the physical transient behavior of the phenomenon and the three-dimensional effects, becoming a very useful design tool in the cases of very complex geometries. The numerical results obtained using Finite Volumes Method matched with experimental results in all points verified.

7. ACKNOWLEDGEMENTS

The authors thank the financial support from CAPES, Brazil, through a master scholarship grant to Carlos E G Falcão, and from CNPq, Brazil, through a scientific productivity grant to Vielmo, H.A. and the CNPq Universal Project 475237/2009-9. . The authors thank FIAT Research Center (CRF-Italy) and Minas Gerais State Research Support Foundation (FAPEMIG), for the financial support to this project.

8. REFERENCES

Al-Falahi Amir, Yusoff M. Z. and Yusaf T., 2010, "Numerical Simulation of Inviscid Transient Flows in Shock Tube and its Validations", International Journal of Mathematical, Physical and Engineering Sciences.

Benson R.S. , 1973 "A comprehensive digital computer program to simulate a compression ignition engine including intake and exhaust systems" – SAE Paper Nº 710173.

Benson R.S. , 1982 "The thermodynamics and gas dynamics of internal combustion engines" Vol.I - Oxford University Press.

Benson R.S., 1986 The thermodynamics and gas dynamics of internal combustion engines Vol. II - Oxford University Press.

Brown J.M.B.; Vardy A.E., 1994, "Reflections of pressure waves at tunnel portals", Journal of Sound Vibration N173 (1).

Hanriot M.S., 2001, "Study of pulsating flow phenomena in air intake ducts in internal combustion engines", Doctorate Thesis, Mechanical Engineering Department, – Pontifical Catholic University of Minas Gerais – PUCMinas – Belo Horizonte, MG, Brazil.

Hirsch, C., Numerical Computation of Internal and External Flows - Vol I e II, 2007, "Fundamentals of Computational Fluid Dynamics", John Wiley & Sons, New York.

Jameson, A., Schmidt, W. and Turkel, E.,1981, "Numerical Solutions of the Euler Equations by Finite Volumes Method using Runge-Kutta Time Stepping Schemes" AIAA Paper No. 81-1259

Morse, P. H., Boden, R. H. e Schecter , H. , 1938, "Acoustic Vibrations and Internal Combustion Engine Performance", Journal of Applied Physics, Vol. 9, January.

Merkle C. L. and Athavale M., "A time accurate unsteady incompressible algorithm based on artificial compressibility". AIAA Conference Paper, 87-1137, 1987.

Sod G.A., 1978, "A survey of several finite difference methods for systems of nonlinear hyperbolic conservation laws", J. Comput. Phys. 43.

Star CCM+ 5.02 User Guide, 2010.

Turkel E., "Preconditioned methods for solving the incompressible and low speed compressible equations" Journal of Computational Physics, 72(2):277–298, 1987.

Turkel E, "Preconditioning techniques in computational fluid dynamics. Annual Review of Fluid Mechanics" 31:385–416, 1999.

Weiss, J.M., Maruszewski, J.P., and Smith, W.A., 1999, "Implicit solution of preconditioned Navier-Stokes equations using algebraic multigrid", AIAA Journal, 37(1), pp. 29-36.

Weiss, J.M., and Smith, W.A., 1995, "Preconditioning applied to variable and constant density flows", AIAA Journal, 33(11), pp. 2050-2057.

William-Louis M.J.P.; Tournier C., 2004, "Numerical and experimental study of transversal pressure waves at a tube exit", Experimental Thermal and Fluid Science.

Winterbone, D.E., Worth, D. and Nichols, J.R., 1989, "A comparison of synthesis and analysis models for wave action manifolds." Proc. Of the ImechE C372/037.

Yasunobu T.; Kuchii S.; Kashimura H.; Setoguchi T., 2002, "Characteristics of compression wave caused by reflection of expansion wave at open end of tube". Journal of Thermal Science Vol.11, No.2.

9. RESPONSIBILITY NOTICE

The authors are the only responsible for the printed material included in this paper.